Doppler optical coherence tomography to monitor the effect of photodynamic therapy on tissue morphology and perfusion

Maurice C. G. Aalders
University of Amsterdam
Academic Medical Center
Laser Center
Meibergdreef 9
1105 AZ, Amsterdam, The Netherlands
and
The Netherlands Cancer Institute
Department of Experimental Therapy
Antoni van Leeuwenhoek ziekenhuis
Amsterdam, The Netherlands
E-mail: M.C.Aalders@amc.uva.nl

Martijn Triesscheijn
Marjan Ruevekamp
The Netherlands Cancer Institute
Department of Experimental Therapy
Antoni van Leeuwenhoek ziekenhuis
Amsterdam, The Netherlands

Martijn de Bruin
University of Amsterdam
Academic Medical Center
Laser Center
Meibergdreef 9
1105 AZ, Amsterdam, The Netherlands

Paul Baas
The Netherlands Cancer Institute
Department of Thoracic Oncology
Antoni van Leeuwenhoek ziekenhuis
Amsterdam, The Netherlands

Dirk J. Faber
University of Amsterdam
Academic Medical Center
Laser Center
Meibergdreef 9
1105 AZ, Amsterdam, The Netherlands

Fiona A. Stewart
The Netherlands Cancer Institute
Department of Experimental Therapy
Antoni van Leeuwenhoek ziekenhuis
Amsterdam, The Netherlands

Abstract. We investigated the feasibility of using optical coherence tomography (OCT) for noninvasive real-time visualization of the vascular effects of photodynamic therapy (PDT) in normal and tumor tissue in mice. Perfusion control measurements were initially performed after administrating vaso-active drugs or clamping of the subcutaneous tumors. Subsequent measurements were made on tumor-bearing mice before and after PDT using the photosensitizer meta-tetrahydroxyphenylchlorin (mTHPC). Tumors were illuminated using either a short drug light interval (D-L, 3h), when mTHPC is primarily located in the tumor vasculature or a long D-L interval (48 h), when the drug is distributed throughout the whole tumor. OCT enabled visualization of the different layers of tumor, and overlying skin with a maximal penetration of $\leq$0.5–1 mm. PDT with a short D-L interval resulted in a significant decrease of perfusion in the tumor periphery, to 20% of pre-treatment values at 160 min, whereas perfusion in the skin initially increased by 10% (at 25 min) and subsequently decreased to 60% of pre-treatment values (at 200 min). PDT with a long D-L interval did not induce significant changes in perfusion. The concept of using noninvasive OCT measurements for monitoring early, treatment-related changes in morphology and perfusion may have applications in evaluating effects of anti-angiogenic or antivascular (cancer) therapy. [DOI: 10.1117/1.2337302]

Keywords: optical coherence tomography; photodynamic therapy; tumor vascular damage.

Paper 05257RR received Sep. 2, 2005; revised manuscript received Mar. 28, 2006; accepted for publication Apr. 3, 2006; published online Aug. 31, 2006.

1 Introduction

Photodynamic therapy (PDT) initiates a photochemical reaction, which causes tumor destruction either by direct tumor cell killing or indirectly via vascular damage and an elicited immune response. For the photochemical reaction to occur, photosensitizer, oxygen, and light must be present in the target area. After administration, the kinetics of the distribution of the photosensitizer are tissue type- and site-dependent. The mechanism of action of PDT depends on both the photosensitizer and on the drug light (D-L) interval.

Address all correspondence to Maurice Aalders, Laser Ctr., Academic Medical Ctr., Meibergdreef 9, Amsterdam 1105 AZ The Netherlands; Tel: +31205663829; Fax: +31206975594; E-mail: M.C.Aalders@amc.uva.nl

1083-3668/2006/11(4)/044011/8/$22.00 © 2006 SPIE

Although the idea of combined vascular and tissue damage is becoming more widely accepted, most clinical protocols for PDT are currently based on the assumption that optimum intervals between photosensitizer administration and illumination relate to the maximum difference between drug uptake in tumor and surrounding normal tissue. However, if vascular mediated tissue damage is the main determinant of tumor destruction, the optimal time interval should be more closely related to high blood plasma drug levels. Although several studies report on the effects of PDT on tissue and vasculature, the relationship between extent of vascular damage and efficacy of treatment is still not fully understood.[1–6] Noninvasive methods that allow studying temporal changes in tissue perfusion following PDT could help to clarify the importance of vascular damage in clinical PDT. They could also serve as an early predictor of the efficacy of treatment.

Optical coherence tomography (OCT) is a high-resolution, cross-sectional imaging to technique that enables noninvasive examination of superficial tissue structures. By combining amplitude and phase-sensitive detection, it is possible to extract the spectral content of the backscattered light. When the light is reflected by a moving particle, the spectrum will acquire a frequency (Doppler) shift. OCT therefore enables cross-sectional imaging of blood flow in superficial vessels, in addition to structural imaging. The clinical use of OCT for imaging of morphological changes following PDT has been described for ophthalmological applications and for monitoring laser surgery of laryngeal carcinoma.[7–10]

In this study, the possibilities and limitations of optical coherence tomography for the assessment of PDT effects will be investigated on both normal and tumor tissue. For validation of the technique, several conditions will be imposed to influence the perfusion in a controlled way. Then, OCT is used to noninvasively obtain real-time information on the development of phototoxic tissue damage following mTHPC-PDT in normal and tumor tissue of mice.

2 Methods

2.1 *OCT Measurement and Signal Processing*

Measurements were performed using a fiber-based time-domain OCT setup with a 1300-nm super luminescent diode (SLD). Light from the SLD was split into two arms by a 50:50 fiber splitter. Longitudinal scanning was obtained by using a tilting mirror (200 Hz) in the rapid scanning optical delay (RSOD) line in the reference arm.[11] Transversal scanning was obtained by scanning the sample with the object beam. Signals at the detector were digitized and processed by a computer to form 2-D tomographic images (512 $\times$1024 pixels, 8$\times$1.4 mm, axial resolution: $\approx$12 μm, lateral resolution $\approx$20 μm).

For the results presented here, 32 consecutive axial samples were used to calculate a frequency spectrum using a Fourier transform algorithm (see Fig. 1). A Gaussian waveform was fitted to the spectrum to obtain a center frequency, amplitude, and spectrum width. The Fourier window was moved over the whole dataset (2-D area). A shift of the center frequency relates to flow or other causes of movement of the sampled volume. To correct for low-frequency motion artifacts, caused by breathing and beating of the heart, the average Doppler shift in a specific depth scan (a-scan) was calculated and subtracted from all values in that a-scan. Noise in the resulting dataset was further reduced by applying a moving average window (5$\times$5 pixels) and a threshold before the Doppler shift image was superimposed on the amplitude picture. The value of the applied threshold, obtained with control measurements described ahead, determined the minimal detectable flow.

Because of the averaging procedures and the unknown angle of the blood vessels with respect to the probing beam, no attempt was made to calculate real flow velocities. The direction of the flow was not taken into account. From the resulting images, the relative perfused area (RPA), which we define as the ratio of the number of pixels indicating perfusion over the total number of pixels in a region of interest, was determined. The values reported here are ratios of the RPA before and after the treatment and therefore represent relative changes in perfusion (RCP).

Where possible, three areas were identified in the images: skin, connective tissue, and tumor periphery. Figure 2 shows an OCT image in relation to a typical histology image of untreated mouse skin and subcutaneous tumor. A grayscale is used to visualize the differences in back scattering; a brighter layer indicates higher back scattering. The upper layers of skin (stratum corneum, epidermis, and dermis) are highly reflecting (area A in Fig. 2). Between the skin and the tumor or muscle, a low reflecting layer can be observed, which consists of loose connective tissue containing blood vessels (area B). Area C is a combination of a thin, highly vascularized muscle layer that is usually distinguishable below the connective tissue layer forming the capsule of the tumor and the upper part of the tumor.

To compare the PDT effects quantitatively, the slope of the backscattered light as a function of depth in the tissue was determined. The attenuation coefficient changes if the viability or configuration of the cells changes.[2] As described by van Leeuwen et al., this slope is a function of both the point spread function (PSF) of the OCT system and the optical properties (attenuation coefficient) of the tissue.[13] We have not determined the PSF of our system but fixed the focus at the air tissue boundary, thereby keeping the influence of the PSF constant throughout the measurements. Furthermore, a low NA lens was used to focus the beam on the tissue, which reduces the influence of the PSF on the signals. The reported values are therefore proportional to the attenuation coefficient and can consequently be used to follow relative temporal changes in tissue morphology.

2.2 *Animals*

Female nude BALB/c mice were used for all experiments. HNXOE cells (kindly provided by G. van Dongen, Vrije Universiteit, Amsterdam, The Netherlands) originated from a human head and neck squamous cell carcinoma metastasis in the oral cavity. HNXOE cells were cultured in Dulbecco modified Eagle medium (Gibco, Rockville, MD) supplemented with 5% fetal calf serum (Gibco) and antibiotics and grown at 37 °C in a 5% CO_2 incubator. To propagate donor tumors *in vivo*, 10^6 HNXOE cells, in a volume of 0.1 ml PBS, were injected subcutaneously in the lower dorsum of mice. When these donor tumors had reached a mean diameter of 8–10 mm, tumor fragments (± 1 mm^3) were transplanted

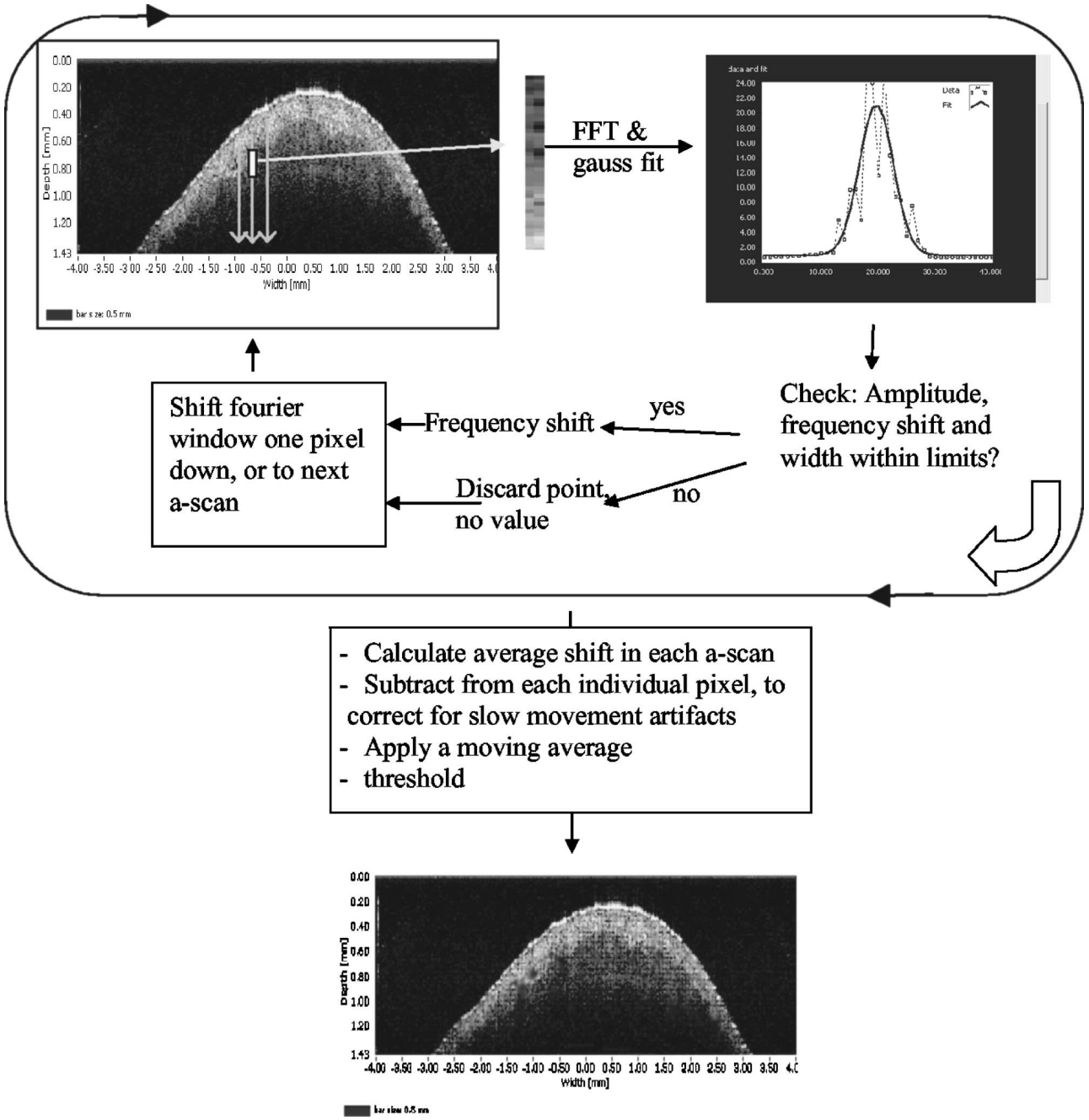

Fig. 1 Measurement scheme. A window of consecutive 32 samples is used to calculate the frequency shift, which is then assigned to the first (top) pixel of that window. Then the window is shifted one pixel down or to the next a-scan and the calculation is repeated. After completion of the last a-scan, the average frequency shift was calculated from all the values in one a-scan. This average value, containing the (low) frequency shift caused by breathing and beating of the heart, was subtracted from all individual values in the a-scan. Then a moving average window and a threshold is applied on the result.

into the lower dorsum of recipient experimental mice. This two-step procedure was used to create well-localized spherical subcutaneous tumors with predictable growth velocity. The time required for the tumor to get to 5–7-mm diameter was about 27 days. During the imaging procedures, the mice were anesthetized by i.p. administration of a mixture of hypnorm and dormicum (12.5 $mg \cdot kg^{-1}$ fluanisol +0.4 $mg \cdot kg^{-1}$ fentanyl citrate and 6.25 $mg \cdot kg^{-1}$ midazolam hydrochloride). To maintain body temperature, a temperature-controlled underlay (37 °C) was used.

2.3 *Control Groups*

Four control groups were used, each comprising two animals. In the first control group, the blood flow in the skin, connective tissue, and tumor was completely blocked by fixing a

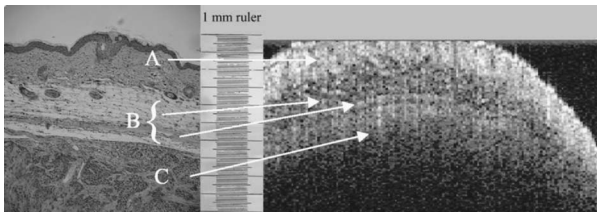

Fig. 2 Histology image of untreated mouse skin with a subcutaneous tumor (left image), a ruler with a total length of 1 mm, and a representative OCT image (different location) is shown on the right image. Three different tissue layers in depth are indicated: A (skin), B (connective tissue), and C (tumor periphery consisting of the capsule and the upper part of the tumor).

metal clamp around the tumor area (see Fig. 3). The effects on flow before, during, and after these interventions were measured by OCT. In groups 2 and 3, vasodilation was induced by administration of 5 mg/kg nicotinic acid (0.75 mg/ml solution) or 300 mg/kg hydralazine (60 mg/ml solution), respectively. Both drugs are vasoactive but have different working mechanisms. A vasodilation in the cutaneous blood vessels, resulting in an increased blood flow, was expected for both drugs. Nicotinic acid was also expected to lead to an improvement in tumor perfusion by preventing temporary shutdown of tumor vessels.[14–17] Hydralazine is known to reduce the peripheral vascular resistance by directly relaxing arteriolar smooth muscle. This causes a relative decrease in perfusion of some tumor types, as the blood flow is preferentially diverted to critical normal tissues; the so-called steal effect.[18,19] In the fourth group, two animals received the photosensitizer but were not illuminated to assess the effect of the drug alone. In one animal of this last group, we imaged a needle that was inserted in the tumor and under the overlying skin. The OCT image was compared with the corresponding histology slide to identify the different layers in our measurement volume (data not shown).

2.4 *PDT Group*

mTHPC (Quanta Nova LTD, Scotland, supplied as a solution, 4 mg/ml drug in a mixture of 1:1:2 propylene glycol:ethanol:water) was administered via the tail vein at a dose of 0.3 mg/kg. At either 3 h or 48 h after administration, the mice were anesthetized, after which the skin of the flank and

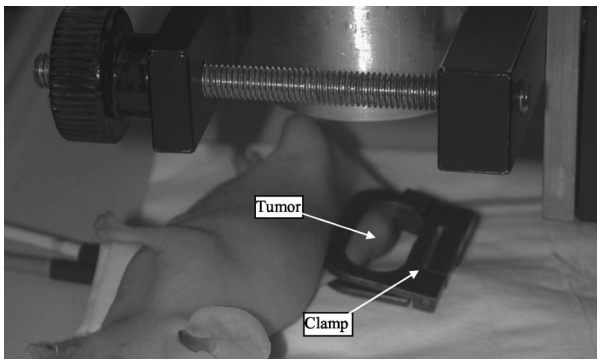

Fig. 3 Mouse under the scanning head of the OCT device, a metal clamp was fixed around the tumor area.

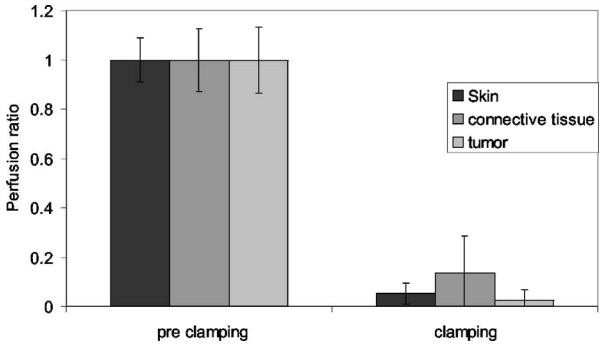

Fig. 4 Effect of placement of a clamp on the perfusion of the skin, connective tissue, and tumor. The results are normalized on the pre-clamping values. The results are means ±SD (3 measurements per mouse, 2 mice per data point).

lower dorsum overlying the tumor was observed by OCT. After these pre-treatment measurements, the animals were illuminated with 100 mW/cm^2 652 nm light. A total energy of 30 J/cm^2 was delivered using a bare fiber. The illumination spot was adjusted to cover the tumor with 0.5-cm margins. Repeated OCT measurements were made for up to 4 hours after illumination. The measurements were done in triplicate (for each time point, on each animal, three independent measurements) and three mice were used in each group. After the last measurement, the animals were sacrificed and tissue samples were collected from both treated and nontreated areas and processed for histology.

2.5 *Ethics*

The study protocol was approved by the local animal welfare committee and conformed to national and European regulations for animal experimentation.

3 Results

3.1 *Control Groups*

OCT measurements made before and 10 minutes after clamping of the tumor and overlying skin (group 1) clearly showed a dramatic drop in RPA after clamping (Fig. 4). Flow immediately-stalled in all three layers. After removal of the clamp, perfusion remained absent in both skin and tumor during the observation period (10 minutes). In the connective tissue layer, however, Doppler shifts above threshold were seen after removal of the clamp.

Perfusion of peripheral areas of the HNXOE xenograft, overlying connective tissue, and skin was also measured repeatedly after administration of nicotinic acid or hydralazine (Fig. 5). Both drugs induced an increase in perfusion in the skin immediately after administration, but changes induced in skin were much more pronounced for nicotinic acid (Fig. 5(a)). As expected, an increase in the tumor perfusion was observed after administration of nicotinic acid and a decrease after administration of hydralazine (Fig. 5(b)). Baseline values of perfusion were restored at 50 minutes and 120 minutes after administration of nicotinic acid and hydralazine, respectively. The same figures (Figs. 5(a) and 5(b)) show the average values of the RPS measured in skin of control group 4

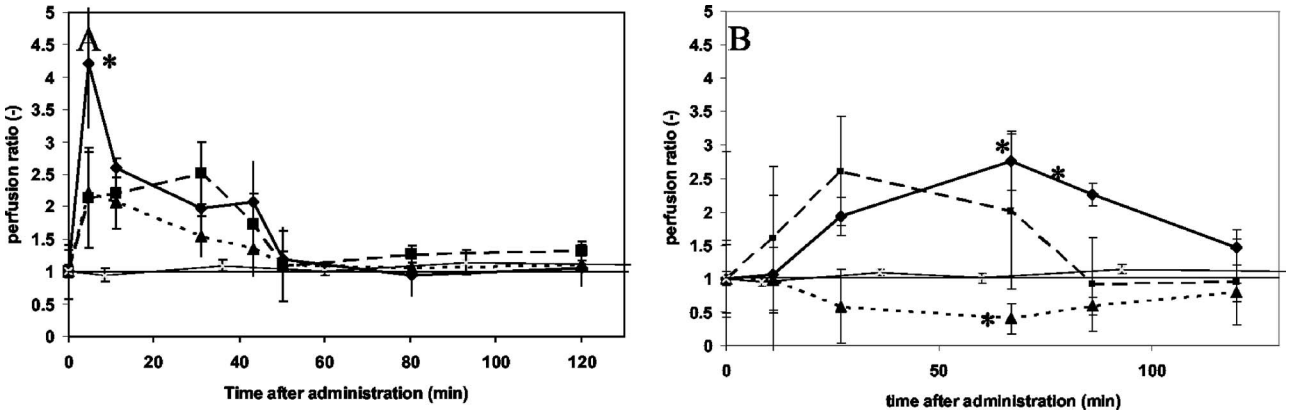

Fig. 5 Perfusion in the mouse skin, connective tissue, and tumor after administration of nicotinic acid [left graph (A)] and hydralazine [right graph (B)]. The * indicates significant differences from baseline values [(t-test, paired, $p<0.05$)]. Legend: –♦–: skin; –■–: connective tissue; |–▲–: tumor; —: control. The results are means ±SD (3 measurements per mouse, 2 mice per data point).

(photosensitizer, no light). No significant changes were observed, which is also true for the RPS in the other layers.

3.2 *PDT Group*

Figure 6 shows the OCT images and corresponding histology before (Fig. 6(a)) and 138 min after PDT (Fig. 6(b)) using a 3 hr D-L interval. The two graphs on the right side show the intensity of the backscattered light as a function of depth.

The most striking histological difference in tissue structure after PDT was the large amount of edema that accumulated in the connective tissue layer (compare Figs. 6(a) and 6(b)). This caused an increase in scattering (see also Fig. 7) and a thickening of the connective tissue layer (Fig. 6(b)), which hampered imaging of the underlying tumor.

Changes in light attenuation after PDT for the 3 hr D-L (A) and 48h D-L (B) interval groups are shown in Fig. 7. All layers showed a trend for increased attenuation after PDT. This was greatest in the peripheral tumor layer for the 3hr D-L interval and greatest in the skin for the 48 hr D-L interval, but none of the individual measurements was signifi-

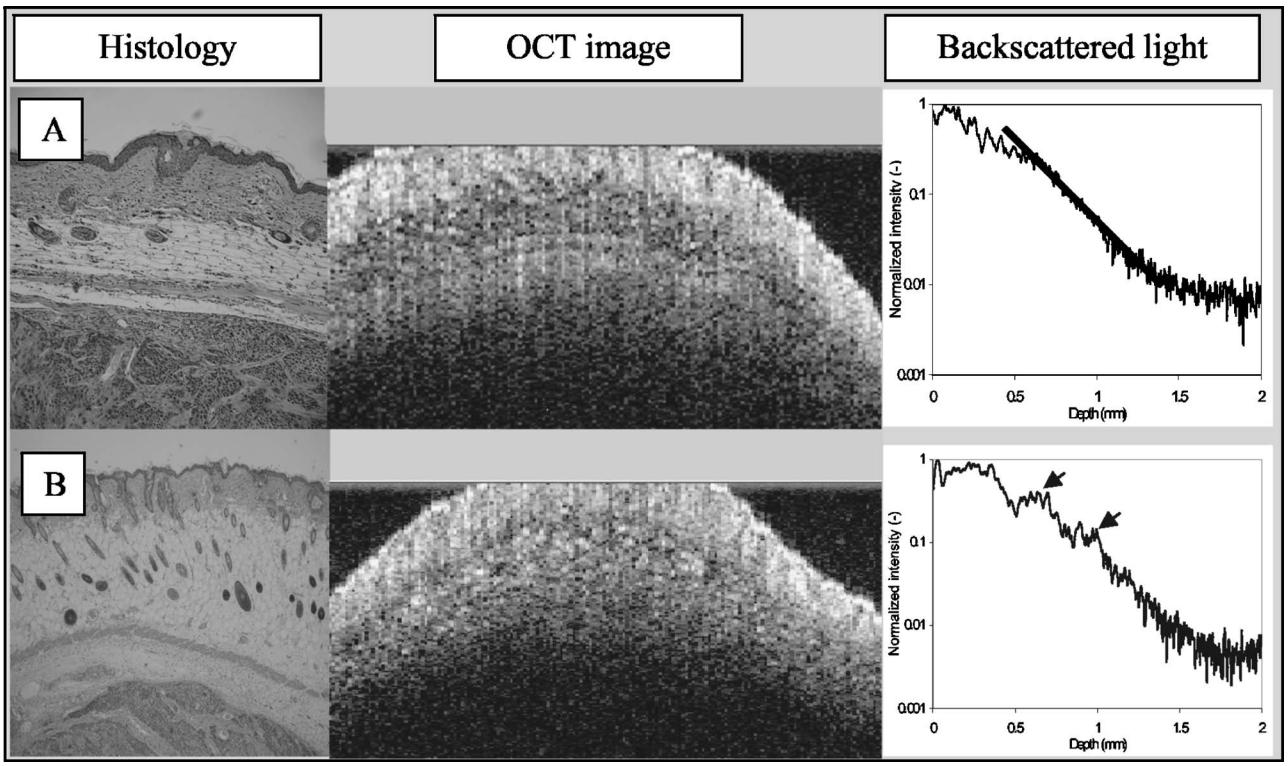

Fig. 6 Histology and OCT image of mouse skin with underlying subcutatious tumor, before treatment (top row, A) and 138 min after treatment (bottom row, B, 3 hr D-L interval) The graphs on the right show the backscattering intensity that was used to calculate the attenuation (see Fig. 6). Depth 0 represents the tissue surface. The arrows show the area of increased backscattering by edema. This causes an increased signal level and a stronger decrease of the signal in depth.

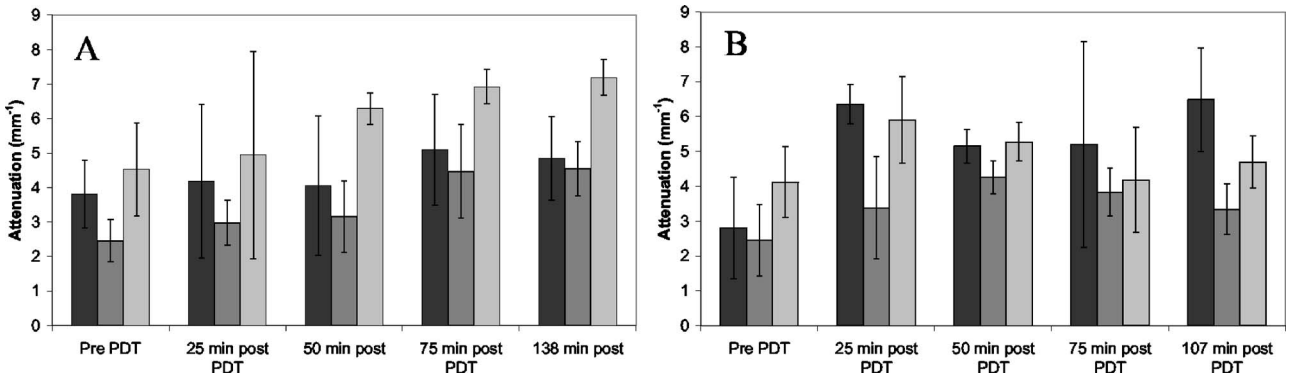

Fig. 7 Optical attenuation (base e) in the different layers at different times after PDT for short (3 hr) D-L interval (5A) and 48 hr D-L interval (5B). ■| skin; ⧈| connective tissue and □: tumor. The results are mean ± SD (3 measurements per mouse, 2 mice per data point).

cantly different from baseline. The large error bars reflect biological variability, inhomogeneities in the layer, and the high sensitivity of the fitting procedure for the length of the segment over which the fit is done.

Changes in RCP with time after PDT are shown in Fig. 8. After PDT with a short D-L interval (3 h) perfusion of skin and tumor periphery decreased to values of 50% (skin) and 30% (tumor) after 160 minutes. Perfusion in the connective tissue initially increased, followed by a decrease in perfusion to a value that was approximately half the baseline value at 160 to 200 minutes. After PDT using longer D-L interval (48 h), no significant changes in RCP were seen.

4 Discussion

The present study shows the possibilities and limitation of optical coherence tomography for the assessment of PDT effects on both normal and tumor tissue. For validation of the technique, several conditions were imposed to influence the perfusion in a controlled way. First the flow was completely stopped in the target area by clamping the tumor and skin. The rapid and complete inhibition of perfusion was used to optimize the algorithms used to extract the flow parameters from the raw data. Next, nicotinic acid or hydralazine were administered to check that tissue layer-dependent changes in perfusion could be followed with OCT.

The OCT tissue images that were taken after PDT showed a clear change in morphology (edema formation) and perfusion. These results were more pronounced for a 3 h D-L interval compared with a 48 h D-L interval. Furthermore, OCT could identify the different layers of tumor and overlying skin, with a maximal penetration of 0.5–1.0 mm in this model. Flow information could be obtained over the full depth range of the structural image. The limited depth penetration represents one of the major limitations of OCT imaging. Motion artefacts in the signal, caused by breathing, heart beat, and muscle twitching were in the order of the local Doppler signal. Because this Doppler shift was usually present in the whole depth scan it could be taken into account in the algorithms and separated from a localized Doppler frequency.

Like ultrasound, OCT provides images that require interpretive skills and training. It is hard to draw conclusions from the images alone. Most toxic processes, e.g., apoptosis and necrosis, cause changes in optical attenuation. By quantifying the signals these processes can be followed in time. The trends in attenuation that we observed suggest treatment-related processes. We have previously shown that in cell suspensions apoptosis caused an increase in scattering while necrosis caused a decrease in scattering.[12] However, in an *in vivo* situation additional processes will influence the attenuation of light, like the influx of edema and a change in blood

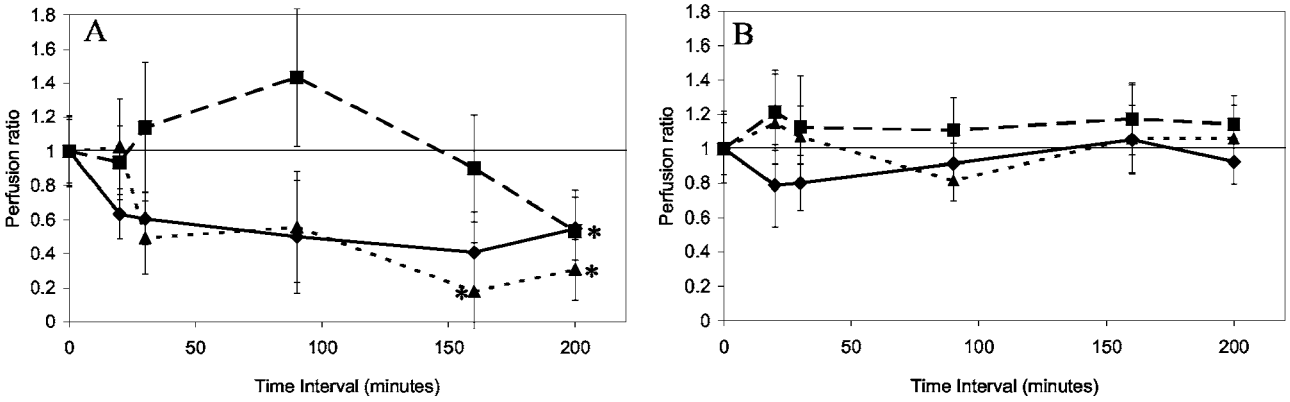

Fig. 8 Perfusion effects in skin, tumor, and connective tissue after PDT for 3- and 48-hr D-L intervals (Figs. A and B, respectively. Error bars indicate SD). The * indicates a significant (t-test, paired, $p<0.05$) difference from baseline values. Legend: –◆–: skin; –■–: connective tissue; |–▲–|: tumor. The results are mean ± SD (3 measurements per mouse, 3 mice per data point).

volume. Further research on this subject is necessary.

Noninvasive imaging of pathologic tissue is preferable to invasive biopsies in many clinical conditions, not only for establishing a diagnosis but also for real-time assessment of treatment-related effects and as guidance during surgery, e.g., for ensuring tumor-free excision edges.

Several factors determine the clinical value of an imaging technique. The clinical value of OCT for the application described in this paper is determined by the imaging resolution, imaging depth, and possibility to assess functional data from the tissue. Considering the first two, for most imaging techniques a trade-off has to be made between imaging depth and resolution. In that respect, OCT can be placed between (fluorescence) confocal microscopy (CM) and high-resolution ultrasound (US).[20–23] CM is capable of visualizing cell layers at micrometer resolution at the cost of a limited penetration depth of around 200 μm. The state-of-the-art ultrasound (70 MHz) currently has resolutions down to 30 micrometer resolution and a penetration depth up to 1 cm.

In addition to CM and US, a number of new technologies are now available for noninvasive optical diagnostic imaging in conjunction with PDT, e.g., MRI, which has a spatial resolution of 0.5–3 mm and is intrinsically sensitive to movement (flow).[24] And, if assessment of perfusion is the main goal, laser Doppler perfusion imaging is an option.[25,26]

The above-mentioned noninvasive techniques are only able to measure average perfusion over a large volume or do not have a high enough resolution to provide any detailed information on PDT effects in specific tissue layers.[27] OCT might overcome these problems due to its high-resolution, depth-resolved measurements. A lot of research has been performed to evaluate the use of OCT to determine functional parameters, like flow, both *in-vitro* and for various clinical applications.[7,28–37] The downside of the technique is obviously the limited penetration of the light. This restricts the clinical use of OCT to superficial tissue layers. In this respect, the mouse model that was used in our experiments turned out to be very challenging. Because of the many strong reflecting layers, it was difficult to extract information from deeper layers in the tissue. Despite this limitation, we were able to follow the phototoxic effect on morphology and perfusion in this particular animal model application, and we may carefully conclude that Fig. 8 suggests that a 3-hr interval may be preferred over a 48-hr interval since there are more pronounced perfusion effects. Our findings justify further exploration of the technique. The concept of using noninvasive OCT measurements for real-time monitoring of morphology and perfusion may have applications in monitoring and optimization of anti-angiogenic or antivascular (cancer) therapy.

Acknowledgments

This study was supported by the Dutch Cancer Society, Grant NKI 2000-2282, and Stichting Dioraphte.

References

1. W. M. Star, H. P. Marijnissen, A. E. van den Berg-Blok, J. A. Versteeg, K. A. Franken, and H. S. Reinhold, "Destruction of rat mammary tumour and normal tissue microcirculation by hematoporphyrin derivative photoradiation observed in vivo in sandwich observation chambers," *Cancer Res.* **46**, 2532–2540 (1986).
2. H. Schouwink, M. Ruevekamp, H. Oppelaar, R. van Veen, P. Baas, and F. A. Stewart, "Photodynamic therapy for malignant mesothelioma: Preclinical studies for optimization of treatment protocols," *Photochem. Photobiol.* **73**, 410–417 (2001).
3. S. Gross, A. Gilead, A. Scherz, M. Neeman, and Y. Salomon, "Monitoring photodynamic therapy of solid tumours online by BOLD-contrast MRI," *Nat. Med.* **9**, 1327–1331 (2003).
4. H. Schouwink, H. Oppelaar, M. Ruevekamp, M. van der Valk, G. Hart, P. Rijken, P. Baas, and F. A. Stewart, "Oxygen depletion during and after mTHPC-mediated photodynamic therapy in RIF1 and H-MESO1 tumours," *Radiat. Res.* **159**, 190–198 (2003).
5. E. Maugain, S. Sasnouski, V. Zorin, F. Guillemin, and L. Bezdetnaya, "Foscan-based photodynamic treatment in vivo: Correlation between efficacy and Foscan accumulation in tumour, plasma and leukocytes," *Oncol. Rep.* **12**, 639–645 (2004).
6. B. Chen, B. W. Pogue, X. Zhou, J. A. O'Hara, N. Solban, N. Demidenko, J. E. Hoopes, and T. Hasan, "Effect of tumour host microenvironment on photodynamic therapy in a rat prostate tumour model," *Clin. Cancer Res.* **15**, 720–727 (2005).
7. A. H. Rogers, A. Martidis, P. B. Greenberg, and C. Puliafito, "Optical coherence tomography findings following photodynamic therapy of choroidal neovascularization," *J. Ophthalmol.* **134**, 566–576 (2002).
8. C. Puliafito, M. R. Hee, C. P. Lin, E. Reichel, J. Schuman, J. S. Ducker, J. A. Izatt, E. A. Swanson, and J. G. Fujimoto, "Imaging of macular diseases with optical coherence tomography," *Ophthalmology* **102**, 217–229 (1995).
9. J. Sahni, P. Stanga, D. Wong, and S. Harding, "Optical coherence tomography in photodynamic therapy for subfoveal choroidal neovascularisation secondary to age related macular degeneration: A cross sectional study," *Br. J. Ophthamol.* **89**, 316–320 (2005).
10. A. V. Shakhov, A. B. Terentjeva, V. A. Kamensky, L. B. Snopova, V. M. Gelikonov, F. I. Feldchtein, and A. M. Sergeev, "Optical coherence tomography monitoring for laser surgery of laryngeal carcinoma," *J. Surg. Oncol.* **77**, 253–258 (2001).
11. G. J. Tearney, B. E. Bouma, and J. G. Fujimoto, "High-speed phase- and group-delay scanning with a grating-based phase control delay line," *Opt. Lett.* **22**, 1811–1813 (1997).
12. F. J. van der Meer, D. J. Faber, R. de Bruin, M. C. Aalders, J. Perree, and T. G. Van Leeuwen, "Changes in optical properties of cells and tissue after induction of apoptosis," *Proc. SPIE* **4431**, 122–125 (2001).
13. T. G. Van Leeuwen, D. J. Faber, and M. C. Aalders, "Measurement of the axial point spread function in scattering media using single mode fiber based optical coherence tomography," *IEEE J. Sel. Top. Quantum Electron.* **9**, 227–233 (2002).
14. D. J. Chaplin, "The effect of therapy on tumour vascular function—invited review," *J. Radiat. Biol.* **60**, 311–325 (1991).
15. D. G. Hirst, B. Joiner, and V. K. Hirst, "Blood flow modification by nicotinamide and metopramide in mouse tumours growing in different sites," *Br. J. Cancer* **67**, 1–6 (1993).
16. A. Rojas, R. J. Hodgkiss, M. R. Stratford, M. F. Dennis, and H. Johns, "Pharmacokinetics of varying doses of nicotinamide and tumour radiosensitisation with carbogen and nicotinamide: Clinical considerations," *Br. J. Cancer* **68**, 1115–1121 (2005).
17. A. Petley, B. Macklin, A. G. Renwick, and T. J. Wilkin, "The pharmacokinetics of nicotinamide in humans and rodents," *Diabetes* **44**, 152–155 (1995).
18. T. Jarm, G. Serša, and D. Miklavèiè, "Oxygenation and blood flow in tumours treated with hydralazine: Evaluation with a novel luminescence-based fiber-optic sensor," *Technol. Health Care* **10**, 363–380 (2002).
19. R. Jirtle, "Chemical modification of tumour blood flow," *Int. J. Hyperthermia* **4**, 355–371 (1988).
20. M. Rajadhyaksha, S. González, J. M. Zavislan, R. R. Anderson, and R. H. Webb, "In vivo confocal scanning microscopy of human skin II: advances in instrumentation and comparison with histology," *J. Invest. Dermatol.* **113**, 293–303 (1999).
21. S. Nori, F. Rius-Díaz, J. Cuevas, M. Goldgeier, P. Jaen, A. Torres, and S. González, "Sensitivity and specificity of reflectance-mode confocal microscopy for in vivo diagnosis of basal cell carcinoma: A multicenter study," *J. Am. Acad. Dermatol.* **51**, 923–930 (2004).
22. C. Harland, J. Bamber, B. A. Gusterson, and P. S. Mortimer, "High frequency, high resolution B-scan ultrasound in the assessment of skin tumours," *Br. J. Dermatol.* **128**, 525–532 (1993).
23. V. Moore and E. Allan, "Pulsed ultrasound measurements of depth and regression of basal cell carcinomas after photodynamic therapy:

Relationship to probability of 1-year local control," *Br. J. Dermatol.*, **149**(5), 1035–1040 (2003).
24. M. O. Leach, "Breast imaging technology: Application of magnetic resonance imaging to angiogenesis in breast cancer," *Breast Cancer Res.* **3**, 22–27 (2001).
25. E. Logean, L. F. Schmetterer, and C. E. Riva, "Optical Doppler velocimetry at various retinal vessel and depths by variation of the source coherence length," *Appl. Opt.* **39**, 2858–2862 (2000).
26. S. Pålsson, L. Gustafsson, N. Bendsoe, M. Soto Thompson, S. Andersson-Engels, and K. Svanberg, "Kinetics of the superficial perfusion and temperature in connection with photodynamic therapy of basal cell carcinomas using esterified and non-esterified 5-aminolaevulinic acid," *Br. J. Dermatol.* **148**, 1179–1188 (2003).
27. A. Jacobssen and G. E. Nilsson, "Prediction of sampling depth and photon pathlength in laser Doppler flowmetry," *Med. Biol. Eng. Comput.* **31**, 301–307 (1993).
28. J. K. Barton, A. J. Welch, and J. A. Izatt, "Investigating pulsed dye laser-blood vessel interaction with color Doppler optical coherence tomography," *Opt. Express* **3**, 251–256 (1998).
29. B. Chen, T. E. Milner, S. Srinivas, X. Wang, A. Malekafzali, M. J. C. van Gemert, and J. S. Nelson, "Noninvasive imaging of in vivo blood flow velocity using optical Doppler tomography," *Opt. Lett.* **22**, 1119–1121 (1997).
30. J. A. Izatt, M. D. Kulkarni, S. Yazdanfar, J. K. Barton, and A. J. Welch, "In vivo bidirectional color Doppler flow imaging of picoliter blood volumes using optical coherence tomography," *Opt. Lett.* **22**, 1439–1441 (2005).
31. L. L. Otis, D. Piao, C. W. Gibson, and Q. Zhu, "Quantifying labial blood flow using optical Doppler tomography," *Oral Surg. Oral Med. Oral Pathol. Oral Radiol. Endod.* **98**, 189–194 (2004).
32. M. C. Pierce, B. H. Park, B. Cense, and J. F. de Boer, "Simultaneous intensity, birefringence, and flow measurements with high-speed fiber-based optical coherence tomography," *Opt. Lett.* **27**, 1534–1536 (2002).
33. T. G. Van Leeuwen, M. D. Kulkarni, S. Yazdanfar, A. M. Rollins, and J. A. Izatt, "High-flow-velocity and shear-rate imaging by use of color Doppler optical coherence tomography," *Opt. Lett.* **24**, 1584–1586 (1999).
34. J. Welzel, C. Reinhardt, E. Lankenau, C. Winter, and H. H. Wolff, "Changes in function and morphology of normal human skin: evaluation using optical coherence tomography," *Br. J. Dermatol.* **150**, 220–225 (2004).
35. S. Yazdanfar, M. D. Kulkarni, and J. A. Izatt, "High resolution imaging of in vivo cardiac dynamics using color Doppler optical coherence tomography," *Opt. Express* **1**, 424–431 (1997).
36. W. Jung, B. Kao, K. M. Kelly, L. H. L. Liaw, J. S. Nelson, and Z. Chen, "Optical coherence tomography for in-vitro monitoring of wound healing after laser irradiation," *IEEE J. Sel. Top. Quantum Electron.* **9**, 222–226 (2005).
37. V. X. D. Yang, J. Pekar, S. S. W. Lo, M. L. Gordon, B. C. Wilson, and I. A. Vitkin, Optical coherence and Doppler tomography for monitoring tissue changes induced by laser thermal therapy—an in vivo feasibility study, *Rev. Sci. Instrum.* **74**, 437–440 (2003).